

Longitudinal Spatial Relationships Between Atrophy and Hypometabolism Across the Alzheimer's Disease Continuum

Jane Stocks^{a,*}, Ashley Heywood^a, Karteek Popuri^{b,c}, Mirza Faisal Beg^b, Howie Rosen^d, Lei Wang^{a,e} and for the Alzheimer's Disease Neuroimaging Initiative¹

^a*Department of Psychiatry and Behavioral Sciences, Feinberg School of Medicine, Northwestern University, Chicago, IL, USA*

^b*School of Engineering Science, Simon Fraser University, Burnaby, Canada*

^c*Memorial University of Newfoundland, Department of Computer Science, St. John's, Canada*

^d*School of Medicine, University of California, San Francisco, CA, USA*

^e*Department of Psychiatry and Behavioral Health, Ohio State University Wexner Medical Center, Columbus, OH, USA*

Handling Associate Editor: Sofia Toniolo

Accepted 7 January 2023

Pre-press 6 February 2023

Abstract.

Background: The A/T/N framework allows for the assessment of pathology-specific markers of MRI-derived structural atrophy and hypometabolism on ¹⁸F-DG-PET. However, how these measures relate to each other locally and distantly across pathology-defined A/T/N groups is currently unclear.

Objective: To determine the regions of association between atrophy and hypometabolism in A/T/N groups both within and across time points.

Methods: We examined multivariate multimodal neuroimaging relationships between MRI and ¹⁸F-DG-PET among suspected non-Alzheimer's disease pathology (SNAP) (A–T/N+; $n = 14$), Amyloid Only (A+T–N–; $n = 24$) and Probable AD (A+T+N+; $n = 77$) groups. Sparse canonical correlation analyses were employed to model spatially disjointed regions of association between MRI and ¹⁸F-DG-PET data. These relationships were assessed at three combinations of time points – cross-sectionally, between baseline visits and between month 12 (M-12) follow-up visits, as well as longitudinally between baseline and M-12 follow-up.

*Correspondence to: Jane Stocks, MS, Department of Psychiatry and Behavioral Sciences, Feinberg School of Medicine, Northwestern University, 710 North Lake Shore Dr. #1303A, Chicago, IL 60611, USA. E-mail: janestocks2018@u.northwestern.edu.

¹Data used in preparation of this article were obtained from the Alzheimer's Disease Neuroimaging Initiative (ADNI)

database (<https://adni.loni.usc.edu>). As such, the investigators within the ADNI contributed to the design and implementation of ADNI and/or provided data but did not participate in analysis or writing of this report. A complete listing of ADNI investigators can be found at: https://adni.loni.usc.edu/wp-content/uploads/how_to_apply/ADNI_Acknowledgement_List.pdf

Results: In the SNAP group, spatially overlapping relationships between atrophy and hypometabolism were apparent in the bilateral temporal lobes when both modalities were assessed at the M-12 timepoint. Amyloid-Only subjects showed spatially discordant distributed atrophy-hypometabolism relationships at all time points assessed. In Probable AD subjects, local correlations were evident in the bilateral temporal lobes when both modalities were assessed at baseline and at M-12. Across groups, hypometabolism at baseline correlated with non-local, or distant, atrophy at M-12.

Conclusion: These results support the view that local concordance of atrophy and hypometabolism is the result of a tau-mediated process driving neurodegeneration.

Keywords: Alzheimer's disease, amyloid, cerebrospinal fluid, magnetic resonance imaging, multimodal imaging, neuroimaging, positron emission tomography, suspected non-Alzheimer's disease pathology, tau

INTRODUCTION

Clinical manifestations of neurodegenerative diseases including Alzheimer's disease (AD) and frontotemporal lobar degeneration (FTLD) are thought to be the result of neurodegeneration in select brain networks that occurs based on the distribution of underlying neuropathology [1]. In line with this view, the "A/T/N" framework [2] has emphasized classifying subjects based on pathology in order to improve antemortem predictions of disease progression [3, 4]. In the A/T/N classification schema, the staging of AD is delineated based on the presence/absence of markers of amyloid- β (A), phosphorylated tau (T), and neurodegeneration (N) in the cerebrospinal fluid (CSF). Thus, subjects are classified into one of multiple possible categories of biomarker abnormality: biomarker "Normal" (BN) for A-T-N-, "Amyloid Only" for A+T-N-, "AD-Continuum" for any A+ category and suspected "Non-AD pathologic change" (SNAP) for any A- with either T+ or N+. In comparison to extensive research delineating the pathological course of AD biomarkers [5-7], consensus on the etiology and the trajectory of SNAP subjects remains unclear [8-12]. It is of critical interest to develop sensitive and specific biomarkers which can differentiate A/T/N groups and provide increased information regarding their longitudinal trajectories.

Imaging measures of structural and functional brain integrity provide an objective and accessible biological means of assessing disease progression *in vivo* [13-16], correlate with clinical and cognitive measures [13, 17, 18], and are sensitive to preclinical disease stages [19]. However, it is currently unclear how the spatial and temporal pattern of multiple measures of neurodegeneration differ among A/T/N groups. Thus, a better understanding of how multimodal signatures vary as a function of pathological syndrome could serve as a valuable biomarker for these groups. In multimodal neuroimaging research,

concordance of imaging modalities refers to the degree to which the signal generated by each modality mirrors the other, and has been used to compare and contrast neuroimaging measures such as atrophy and hypometabolism [20-24]. In particular, Sintini and colleagues [22] examined individuals with atypical clinical phenotypes of AD and found that tau-PET measures showed strong correlations with local (i.e., spatially contiguous) neurodegeneration (e.g., ^{18}F FDG-PET hypometabolism), suggesting tau may be the driving force behind neurodegeneration in this unique cohort. However, many of these studies measured concordance across the whole brain [21] or locally at the level of lobe [20] or network [24], thus providing only a limited description of the link between structure and function in the brain given that functionally connected yet spatially distributed brain regions can be affected by neuropathology [25].

Although they are not specific markers of neurodegenerative pathology, structural MRI-derived measures of cortical atrophy and ^{18}F FDG-PET hypometabolism are routinely used as biomarkers of neurodegeneration [26-28]. Importantly, atrophy and ^{18}F FDG-PET hypometabolism may overlap in critical "hub" regions of functional networks [29], which could serve as key drivers of disease. Moreover, progression of abnormalities in measures of brain structure and function occurs in an unequal temporal and spatial pattern within the brain [30]. Indeed, different pathophysiological aspects of neurodegenerative disorders can be captured by different neuroimaging modalities [31]. Further, the cortical pattern of structural and functional changes is not yet well understood among SNAP subjects, and no study to date has directly compared both the cross-sectional and longitudinal relationships between neuroimaging measures among A/T/N groups.

Here, we aimed to determine the relationship between atrophy and hypometabolism in A/T/N

groups both within and across time points. Further, we employed methods to elucidate either local or distant (i.e., spatially disjointed) relationships, allowing insights into both the spatial and temporal patterning of neurodegeneration in A/T/N groups across time. To do so, we implemented sparse canonical correlation analysis (SCCA), an unsupervised multivariate method that estimates the linear relationship between two data sets. SCCA has been implemented previously in neuroimaging studies to compute spatially disjointed associations between modalities [22, 32, 33]. We hypothesized that within time point concordance of atrophy and hypometabolism, as assessed by the SCCA, would be more spatially overlapping than cross-time point canonical dimensions. Cross time-point concordance, in particular baseline ^{18}F FDG-PET to 1-year follow-up atrophy, would be the least spatially overlapping (i.e., spread across brain regions), given the hypothesis that alternations in ^{18}F FDG-PET occur early due to synaptic activity disruptions that subsequently project trans-synaptically to downstream regions resulting in atrophy [34]. Further, due to the supposed regional effects of tau pathology on neurodegeneration, tau-positive groups (SNAP, Probable AD) would show the most spatially overlapping relationships of atrophy and hypometabolism, as compared to Amyloid-Only subjects.

METHODS

Participant selection

Data used in the preparation of this article were obtained from the Alzheimer's Disease Neuroimaging Initiative (ADNI) database (<https://adni.loni.usc.edu>). ADNI was launched in 2003 as a public-private partnership, led by principal investigator Michael W. Weiner, MD. The primary goal of ADNI has been to test whether serial MRI, PET, other biological markers, and clinical and neuropsychological assessment can be combined to measure the progression of AD. Full details of subject recruitment, scanning protocols, diagnostic criteria, as well as imaging and CSF data processing are available on <https://www.adni-info.org>. ADNI protocols can further be found in reports by Jack et al. [35] and Mueller et al. [36]. Procedures involving experiments on human subjects are done in accord with the ethical standards of the Committee on Human Experimentation of the institution in which the experiments were done. ADNI participants were included in the current study when CSF,

structural MRI and ^{18}F FDG-PET data were available at baseline visit and structural MRI and ^{18}F FDG-PET data were available at Month-12 (M-12) follow-up visit.

CSF samples were analyzed at the University of Pennsylvania, according to procedures as described in the ADNI procedures manual (<https://www.adni-info.org/>) using Elecsys CSF immunoassays. Amyloid deposition in the brain is associated with decreased levels of amyloid- β_{1-42} peptide (A β) in the CSF, while high levels of tau protein phosphorylated at threonine 181 (p-tau) in CSF are related to tau aggregation in the brain [37]. Measures of CSF total tau (t-tau) are considered a marker of non-AD specific neurodegeneration [38]. Participants were designated into A/T/N groups based on positive or negative A, T, or N status, using published cut-off points [39]: amyloid positivity (i.e., A+/A-) was based on an A β_{1-42} cut-off of <977 pg/mL; tau positivity (i.e., T+/T-) was based on a p-tau cut-off of >23 pg/ml; neurodegeneration positivity (i.e., N+/N-) was based on t-tau cut-off of >213 pg/ml. Consequently, we designated four A/T/N groups: "Biomarker Normal" (BN) who were A-T-N-, "SNAP" who were Amyloid-negative (A-T-N+, A-T+N-, and A-T+N+), "Amyloid-Only" who were only positive for only A β (i.e., A+T-N-), and "Probable AD" who were positive for A β , t-tau, and p-tau (A+T+N+).

Image processing

Structural MRI

Detailed descriptions of the ADNI image acquisition protocols procedures and post-acquisition preprocessing procedures can be found at <https://www.adni.loni.usc.edu>. This included geometric distortion of gradient nonlinearity, non-uniformity normalization, and histogram-peak sharpening, resulting in image volumes at $1 \times 1 \times 1 \text{ mm}^3$ uniform resolution. After downloading from ADNI database, all T1-weighted MRI scans were processed through FreeSurfer version 5.3 [40] to generate cortical surface and thickness measures. Images were then subjected to quality control by visual inspection and any erroneous segmentation was corrected according to FreeSurfer data troubleshooting protocol. Manual correction was repeated until data were deemed ready to use by manual segmentation experts, and any scans noted to contain large or immutable errors were excluded. Cortical thickness was estimated as the

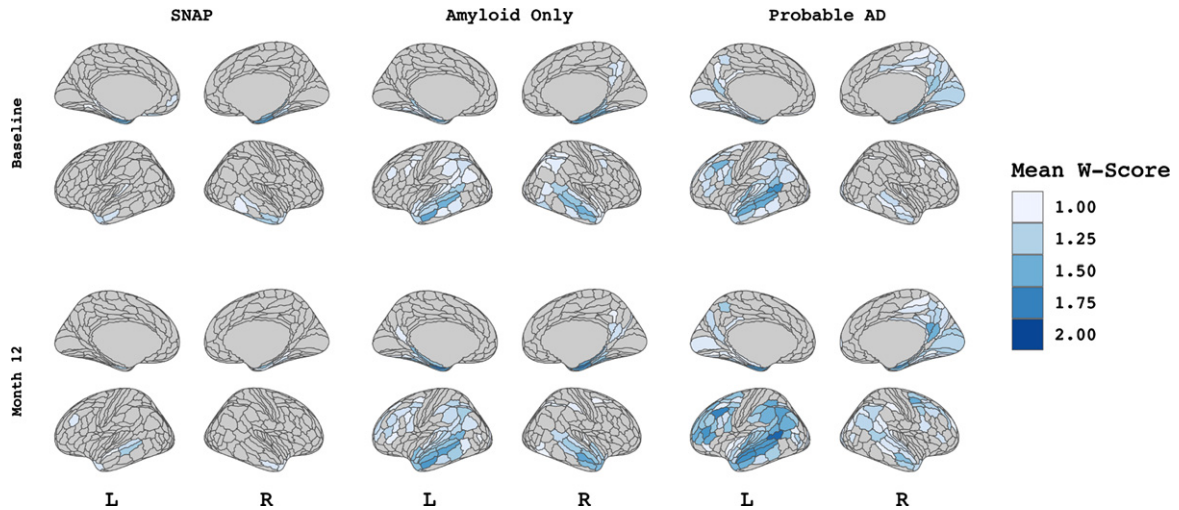


Fig. 1. Patterns of cortical atrophy among A/T/N groups. Figure showing W-score values for each A/T/N group at both baseline visit (upper panel) and M-12 follow-up visit (lower panel). Values indicate the mean W-score within each of 360 patches (HCP-MMP1 atlas) per group thresholded at values greater than 1 to demonstrate atrophy that differs from expected trajectory based on age.

distance between white matter and pial matter at each vertex. To match intrinsic smoothness of ^{18}F FDG-PET images, a 14-mm FWHM kernel was applied to the cortical GM thickness data along the cortical white surface [41]. Cortical thickness values obtained through FreeSurfer were then mapped onto a MNI152 non-linear average (i.e., template white surface), resulting in per-subject thickness maps containing 297,800 vertices across all subjects for statistical analysis and visualization.

^{18}F FDG-PET

Detailed ADNI pre-processing steps for ^{18}F FDG-PET images can be found at <https://adni.loni.usc.edu/methods/PET-analysis/pre-processing>. These included co-registration, averaging, standardizing the spatial resolution, orientation, and normalization, as well as scanner-specific smoothing to achieve a uniform smoothing level of isotropic 8 mm FWHM. After downloading images from ADNI, ^{18}F FDG-PET images were then co-registered with their respective MRI images using the FSL-FLIRT program [42] based on normalized mutual information, using 9 degrees of freedom and normalized correlation as cost function. Cortical ^{18}F FDG-PET uptake values were then re-indexed to the above mentioned MNI-152 template white surface, resulting in corresponding vector sets of cortical ^{18}F FDG-PET uptake values across all subjects for statistical analysis and visualization. To achieve the same effective smoothness for ^{18}F FDG-PET data as with

the cortical thickness processing of 14-mm FWHM, we determined the initial smoothness of the cortical ^{18}F FDG-PET uptake on the surface and performed additional smoothing [43]. The above MRI and ^{18}F FDG-PET image processing steps resulted in multimodal vectors of cortical gray matter thickness and cortical gray matter ^{18}F FDG-PET uptake data smoothed to the same degree across all subjects and correspondingly indexed over the MNI152 non-linear average template white surface.

Generation of vertex- and patch-wise W-score maps

After the above processing steps, W-scores [44, 45] were computed for cortical thickness and ^{18}F FDG-PET uptake to adjust for the effects of normal aging (Fig. 1A). W-scores were calculated by fitting a general linear model (GLM) in a set of reference subjects against age, then taking the standardized residuals generated from this model for all subjects [46]. They are analogous to z-scores, reflecting standardized levels of atrophy and hypometabolism for each individual subject after age-adjustment. For the reference set, we used subjects without a clinical diagnosis who remained cognitively normal through the ADNI follow-up period (see [47] for further details). Vertex-wise W-scores were then calculated for cortical thickness and ^{18}F FDG-PET uptake for all subjects following the formula: $[(\text{subject's raw value}) - (\text{subject's expected value})] / (\text{standard deviation of the residuals in the reference set})$. Finally, cortical surface

vertices were parcellated into 360 roughly-equal-sized patches according to a validated atlas from the Human Connectome Project [48]. Patch-wise cortical thickness and ^{18}F FDG-PET W-scores were obtained by averaging W-scores across all vertices within a patch and used in subsequent sparse canonical correlation analyses. For supplemental analyses, W-scores for atrophy and hypometabolism were also entered into patch-wise direct comparisons using *t*-tests assuming unequal variances. Significance of T-scores was corrected for multiple comparisons using the Benjamini-Hochberg false discovery rate (FDR) of 0.05.

Multivariate sparse canonical correlation analysis

SCCA is an unsupervised multivariate method that estimates the linear relationship designed to take maximal advantage of the correlation among multivariate random variables [49]. Here, SCCA was applied using the penalized multivariate analysis (PMA) R package [50] to examine the relationships between baseline hypometabolism and atrophy, between M-12 hypometabolism and atrophy, and between baseline hypometabolism and M-12 atrophy, within each ATN group. In each analysis, a sparsity lasso penalty of 0.3 for both ^{18}F FDG-PET and MRI data was used, consistent with prior investigations [22, 32]. We applied permutation testing [22, 33] with 10,000 permutations to assess the significance of identified canonical relationships, wherein the *p*-value was defined as the ratio between the number of permutations that resulted in an equal or higher correlation than the original correlation and the total number of permutations applied. Due to the number of SCCAs performed across groups, significance was adjusted using the Benjamini-Hochberg FDR of 0.05. The first canonical dimension, which had 72 (out of 360) patches with non-zero weights, was used for visualization as a color map on the overall average surface using the R package ggseg [51]. Finally, we calculated a Dice spatial overlap between the non-zero patches between atrophy and hypometabolism for further interpretation, using the R package philentropy [52].

Relationship of SCCA regions to cognitive change

We assessed whether the neuroimaging features selected by the SCCA were related to changes in cognition. Cognition was assessed using a composite

scale for memory, ADNI-Mem, [53] extracted from the ADNI neuropsychological battery. The 1-year rate of change in ADNI-Mem was modeled using a linear mixed effects model with fixed effects of time, age, sex, years of education and *APOE* $\epsilon 4$ genotype status with random slope and intercept terms for each participant. The rate of change in cognition for each individual was extracted from the model. Rates of change were then regressed against the mean W-score within the set of patches selected by the SCCA for each modality within each ATN group. Significance was adjusted for multiple comparisons using Benjamini-Hochberg correction for a false discovery rate of 0.05.

RESULTS

Participants

The demographics and clinical characteristics of the study population are listed in Table 1. Differences in study variables were assessed among A/T/N groups using chi-square tests for categorical variables and analyses of variance (ANOVAs) with follow-up pairwise comparisons for continuous variables. Data from 135 subjects with both baseline and M-12 visits from the ADNI database were included in this study. The “Biomarker Normal” (BN) group had 20 subjects, the “SNAP” group had 14 subjects, the “Amyloid Only” had 24, and the “Probable AD” group had 77. There were no significant differences between groups in age or sex. The Probable AD group showed greater frequency of *APOE* $\epsilon 4$ carriers than BN, SNAP, and Amyloid Only ($p < 0.05$), while Amyloid Only showed greater *APOE* $\epsilon 4$ carriership frequency than SNAP ($p < 0.01$). The Probable AD group had lower MMSE and ADNI-Mem score and a higher Clinical Dementia Rating Scale Sum of Boxes (CDRSB) score compared to BN, SNAP, and Amyloid Only subjects (all $p < 0.05$). Probable AD group showed a higher frequency of individuals with a clinical diagnosis of dementia than compared to BN, SNAP, and Amyloid Only subjects (all $p < 0.001$).

Patterns of cortical atrophy and hypometabolism among A/T/N groups

Figure 1 displays vertex-wise patterns of cortical atrophy among the three A/T/N groups at baseline and M-12 visits. Group average W-scores were thresholded at values greater 1 to visualize atrophy that

Table 1
Demographic characteristics

ATN Group	Biomarker Normal (n=20)	SNAP (n=14)	Amyloid Only (n=24)	Probable AD (n=77)	p
Age	76.4 (4.0)	77.5 (7.5)	75.0 (4.9)	74.4 (7.4)	ns
Sex (M/F)	13/7	9/5	17/7	48/29	ns
Education	15.9 (3.2)	16.2 (2.6)	16.1 (2.4)	16.0 (3.1)	ns
APOE ε4 (Y/N)	5/15	1/13	12/12 ¹	56/21 ¹	<0.001
MMSE	28.6 (1.7)	27.60 (1.9)	26.86 (2.4)	25.85 (1.8) ¹	<0.001
ADNI-Mem (bl)	0.48 (0.7)	0.35 (0.9)	0.08 (0.9) ¹	-0.40 (0.6) ¹	<0.001
Slope, ADNI-Mem	0.01 (0.04)	-0.03 (0.03)	-0.06 (0.06)	-0.11 (0.06) ¹	<0.05
CDR-SB	0.58 (0.8)	1.25 (1.2) ¹	1.56 (1.6) ¹	2.55 (1.9) ¹	<0.001
ATN	20 A-T-N-	11 A-T+N+ A-T-N+	24 A+T-N-	77 A+T+N+	-
Clinical Diagnosis (CN/MCI/Dementia)	12/8/0	4/8/2	8/12/4	3/4/30 ¹	<0.001

Table showing summary of demographic variables. Results are reported as mean (std) for continuous variables or counts for discrete variables. ¹indicates $p < 0.5$ for *post-hoc* pairwise analyses versus Biomarker Normal. Age and education are reported in years. MMSE, Mini-Mental State Exam; Memory Composite, Alzheimer's Disease Neuroimaging Initiative Memory Composite; CDRSB, Clinical Diagnostic Rating Scale Sum of Boxes; CN, cognitively normal; MCI, mild cognitive impairment.

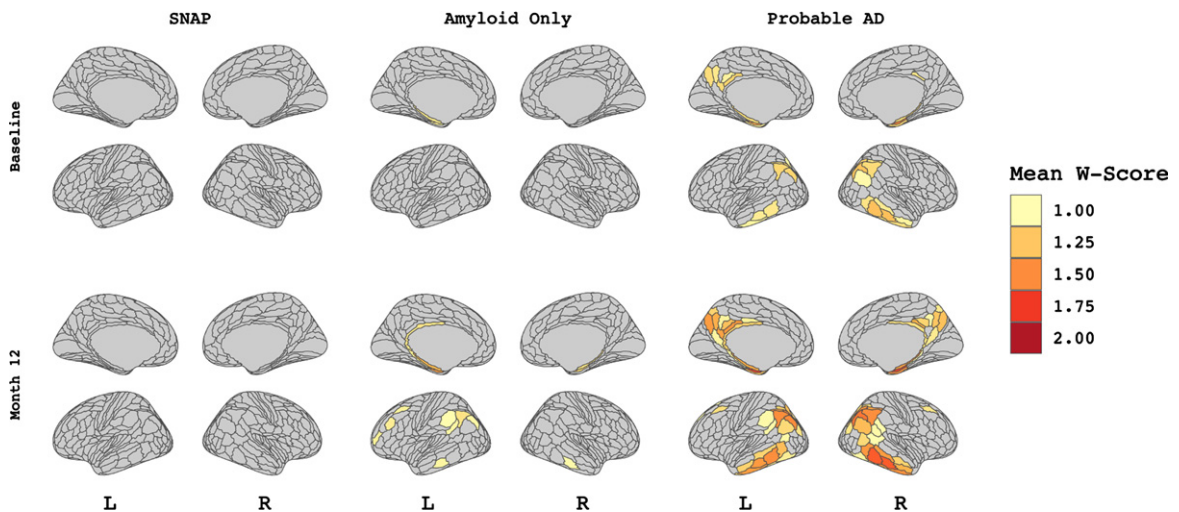


Fig. 2. Vertex-wise patterns of FDG-PET hypometabolism among A/T/N groups. Figure showing vertex-wise W-score values for each A/T/N group at both baseline visit (upper panel) and M-12 follow-up visit (lower panel). Values indicate the mean W-score within each of 360 patches (HCP-MMP1 atlas) per group thresholded at values greater than 1 to demonstrate hypometabolism that differs from expected trajectory based on age.

differed from the expected value based on age. Qualitatively, cortical atrophy among the SNAP group was minimal at both baseline and M-12. However, a small amount of atrophy can be seen in the medial temporal regions at baseline that was relatively stable across time. Among Amyloid Only subjects, there is also evidence of temporal lobe atrophy at baseline, with additional atrophy in the inferior parietal and posterior cingulate cortex, then extends to include

the bilateral middle temporal gyrus at M-12. Probable AD subjects show a characteristic pattern of medial temporal atrophy at baseline, expanding to the inferior parietal, precuneus, and dorsolateral frontal cortex at M-12.

Figure 2 displays patterns of cortical hypometabolism in the three A/T/N groups at baseline and M-12. Qualitatively, mild ¹⁸F-DG-PET hypometabolism was observed in the SNAP subjects

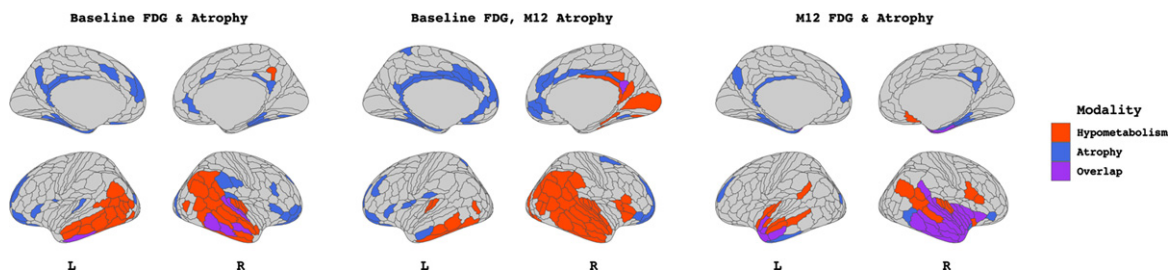


Fig. 3. Output from sparse canonical correlation analyses performed within the SNAP group ($n=14$) between baseline FDG-PET hypometabolism and baseline atrophy W-scores (left), between baseline FDG-PET hypometabolism and M-12 atrophy W-scores (middle), and between M-12 FDG-PET hypometabolism and M-12 atrophy W-scores (right). Patches filled in red and blue represent those which contribute to the canonical dimension from FDG-PET hypometabolism and atrophy, respectively. Patches filled in purple represent those which contribute to the canonical dimension from both modalities. Patch demarcation corresponds to HCP-MMP1 atlas.

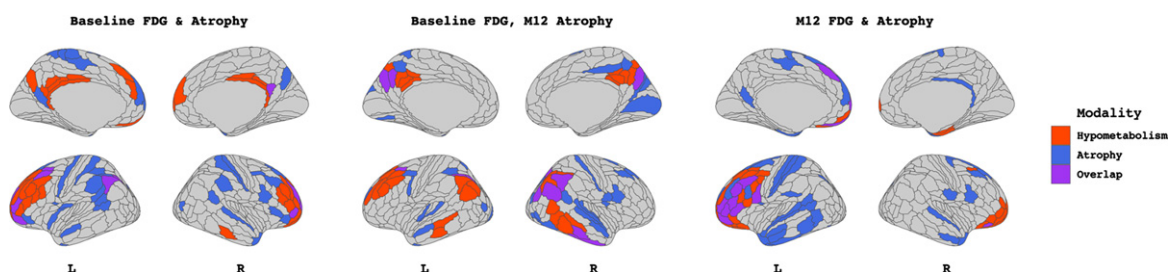


Fig. 4. Output from sparse canonical correlation analyses performed within the Amyloid Only group (A+T-N-, $n=24$) between baseline FDG-PET hypometabolism and baseline atrophy W-scores (left), between baseline FDG-PET hypometabolism and M-12 atrophy W-scores (middle), and between M-12 FDG-PET hypometabolism and M-12 atrophy W-scores (right). Patches filled in red and blue represent those which contribute to the canonical dimension from FDG-PET hypometabolism and atrophy, respectively. Patches filled in purple represent those which contribute to the canonical dimension from both modalities. Patch demarcation corresponds to HCP-MMP1 atlas.

in the dorsolateral frontal and temporoparietal regions at both baseline and M-12. Amyloid Only subjects showed left-hemisphere predominant hypometabolism in the dorsolateral prefrontal and inferior parietal lobule at M-12 only, with minimal hypometabolism at baseline. Hypometabolism in Probable AD subjects follow a canonical temporoparietal-predominant pattern at both baseline and M-12. T-scores directly comparing levels of atrophy and hypometabolism in each A/T/N group at baseline and M-12 are available in Supplementary Figure 1. T-scores are visualized as colormaps where red indicates greater hypometabolism than atrophy and blue indicates greater atrophy than hypometabolism, after controlling for multiple comparisons at an FDR of <0.05 .

Multivariate sparse canonical correlation

The BN group did not show any significant association between atrophy and ^{18}F FDG-PET hypometabolism in any time point combinations. Significant relationships for the SNAP group are dis-

played in Fig. 3. Each panel displays the patches which contributed to the first canonical dimension from hypometabolism (red), atrophy (blue), or both (purple). Visual inspection revealed an association ($p < 0.01$) between baseline atrophy in the bilateral prefrontal, left precuneus, and inferior temporal gyrus with baseline hypometabolism in temporoparietal regions, with a Dice correlation (i.e., degree of spatial overlap) of 0.25. There was a significant ($p < 0.05$) association between baseline hypometabolism in the right temporal lobe to bilateral frontal pole and cingulate atrophy at M-12, with minimal overlap (Dice correlation 0.02). Finally, the relationship between baseline hypometabolism and atrophy at M-12 was significant ($p < 0.001$) with a high degree of spatial overlap (Dice = 0.56), concentrated in the bilateral (right > left) temporal lobe.

Significant relationships for the Amyloid Only group are displayed in Fig. 4. Baseline atrophy throughout the frontal, parietal and temporal lobe and bilateral prefrontal cortical hypometabolism were significantly associated ($p < 0.01$). Overlap was observed in the right inferior parietal lobule (IPL),

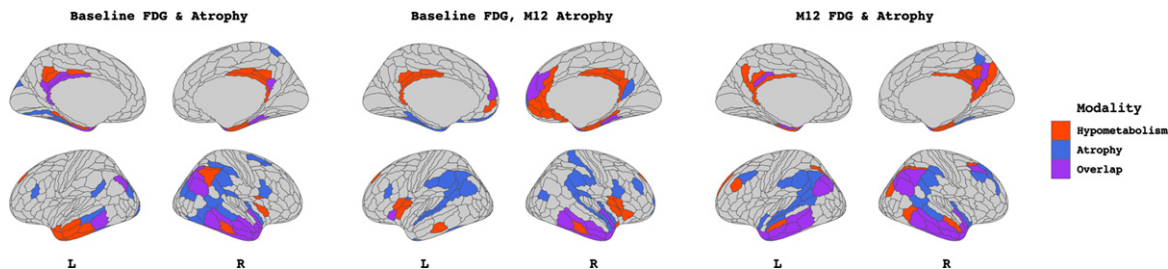


Fig. 5. Output from sparse canonical correlation analyses performed within the Probable AD (A+T+N+, $n = 77$) group ($n = 24$) between baseline FDG-PET hypometabolism and baseline atrophy W-scores (left), between baseline FDG-PET hypometabolism and M-12 atrophy W-scores (middle), and between M-12 FDG-PET hypometabolism and M-12 atrophy W-scores (right). Patches filled in red and blue represent those which contribute to the canonical dimension from FDG-PET hypometabolism and atrophy, respectively. Patches filled in purple represent those which contribute to the canonical dimension from both modalities. Patch demarcation corresponds to HCP-MMP1 atlas.

Table 2
Regression Analyses Predicting Slope of ADNI-Mem

Group	Variable	B [95% CI]	β	SE	Adj R ²	t	p
SNAP	Baseline– Baseline						
	FDG-PET Hypometabolism	0.02* [0.00–0.03]	0.19	0.00	0.30	(2,12) 2.62	0.03
	Atrophy	0.02* [0.00–0.03]	0.16	0.00	0.31	(2,12) 2.72	0.03
	Baseline - M12						
	FDG-PET Hypometabolism	0.02** [0.00–0.03]	0.19	0.00	0.44	(2,12) 3.44	<0.01
Amyloid Only	Baseline– Baseline						
	FDG-PET Hypometabolism	0.00 [–0.01–0.01]	0.07	0.01	–0.04	(2,22) 0.17	<i>ns</i>
	Atrophy	0.00 [–0.01–0.01]	0.06	0.01	–0.04	(2,22) 0.04	<i>ns</i>
	Baseline - M12						
	FDG-PET Hypometabolism	–0.01 [–0.02–0.00]	0.03	0.01	–0.03	(2,22) –0.37	<i>ns</i>
Probable AD	Baseline– Baseline						
	FDG-PET Hypometabolism	0.01* [0.00–0.03]	0.17	0.00	0.14	(2,75) 2.02	0.04
	Atrophy	0.01 [–0.01–0.02]	0.05	0.00	0.02	(2,75) 1.54	<i>ns</i>
	Baseline - M12						
	FDG-PET Hypometabolism	0.02* [0.00–0.03]	0.23	0.00	0.16	(2,75) 2.17	0.03

* $p < 0.05$. ** $p < 0.01$. Multiple comparisons correction applied: FDR.

left precuneus, and right inferior temporal gyrus at a Dice correlation of 0.12. A significant relationship ($p < 0.05$) was observed between baseline hypometabolism within the bilateral IPL, precuneus and frontal cortex and diffuse atrophy at M-12 in the temporal, parietal and occipital regions, with an overlap Dice correlation of 0.28. At month-12, hypometabolism in the frontal pole and orbitofrontal cortex correlated and atrophy in the dorsolateral prefrontal (DLPFC) as well as anterior temporal regions showed a significant association ($p < 0.01$), with an overlap Dice correlation of 0.28.

Figure 5 displays significant relationships in the Probable AD group significant (all $p < 0.001$). Atrophy-hypometabolism SCCA at baseline showed a high degree of spatial overlap (Dice = 0.45), concentrated in the bilateral temporal lobes for both atrophy and hypometabolism. Baseline hypometabolism in

the right temporal and anterior and posterior cingulate cortices correlated with bilateral temporoparietal/IPL atrophy at M-12, with an overlap Dice correlation of 0.29. M-12 analysis revealed a high degree of overlap (Dice 0.50) between hypometabolism and atrophy, concentrated in the temporoparietal cortices.

Relationships to cognition

In the SNAP group, baseline ¹⁸FDG-PET hypometabolism was correlated to the slope of cognitive change (i.e., hypometabolism was related to declining cognition) within the patches identified as correlated to both baseline and M-12 atrophy (all $p < 0.05$, Table 2). Atrophy at baseline within patches identified as correlated to baseline hypometabolism was correlated to negative slope of cognitive change (i.e., cortical thinning was related

to declining cognition, $p < 0.05$). Among Amyloid Only subjects, neither hypometabolism nor atrophy in SCCA-derived regions at any time point showed a significant relationship to cognitive change (all $p > 0.05$). In Probable AD, hypometabolism at baseline within patches identified as correlated to baseline and M-12 atrophy showed a significant relationship to negative slope of cognitive change (all $p < 0.05$).

DISCUSSION

In this study, we investigated local and distant relationships between atrophy and hypometabolism, both cross-sectionally and longitudinally, across the AD continuum [2]. To do so, we implemented novel multivariate SCCA methodology and applied it to both within- and across-time point data. We showed that, in SNAP subjects, while at the group level there were only minimal deviations from age-expected patterns of atrophy and hypometabolism, a pattern of bilateral temporal lobe hypometabolism at baseline correlated with spatially distant atrophy at baseline as well as at M-12 follow-up. At M-12, however, spatially overlapping relationships between atrophy and hypometabolism in the bilateral (right > left) temporal lobes were observed. Additionally, we observed that Amyloid Only subjects, who showed only mild deviations from age-expected patterns of atrophy and hypometabolism at the group level, showed atrophy-hypometabolism relationships which were generally spatially contiguous (i.e., proximal but not directly spatially overlapping, Dice ranged from 0.24–0.28) both within and across time-points. We found that Probable AD subjects, who showed characteristic patterns of significant deviations from age-expected patterns of atrophy and hypometabolism in the temporoparietal cortex, also showed highly spatially overlapping relationships between atrophy and hypometabolism (Dice ranged 0.29–0.50), concentrated in the bilateral temporal lobes at all time points assessed. Additionally, patterns across the time points showed the least amount of overlap, i.e., when baseline ^{18}F FDG-PET hypometabolism was correlated with atrophy at M-12 follow-up, in particular for the SNAP (Dice = 0.02) and Probable AD groups (Dice = 0.29). Overlaps were generally low in Amyloid Only subjects at all time points assessed (Dice ranged from 0.24–0.28), possibly reflecting the aforementioned spatially contiguous relationships between the patches contributing to the canonical dimensions among this group. Finally, we

showed that ^{18}F FDG-PET hypometabolism in regions identified by the SCCA were correlated to subjects' longitudinal rates of cognitive change in the SNAP and Probable AD groups, while atrophy in regions identified by the SCCA showed similar relationships to cognition only within the SNAP group.

In typical AD-related neuropathological change, alterations in brain glucose metabolism begin in the posterior cingulate cortex before spreading to the neighboring precuneus and temporoparietal cortical areas [54–57]. In contrast, atrophy typically begins in the medial temporal lobe and extends later into the lateral temporal lobes, cingulate cortex, and temporoparietal regions [58–61]. Generally, cortical hypometabolism is observed to be more widespread than atrophy until late in the disease process [23, 44, 45, 62, 63]. Further, patterns of regional alterations in hypometabolism are often topographically distinct from those of atrophy [20, 64]. Explanatory theories with regard to the discrepancy between the topology of atrophy and hypometabolism include that hypometabolism is thought to reflect early synaptic dysfunction that precedes atrophy [65, 66], or that hypometabolism more closely reflects tau pathology due to stronger observed relationships of local hypometabolism to tau-PET [67–71]. Alternatively, it has been posited that FDG-PET hypometabolism can occur in regions that are physically distant, but functionally connected, to a structural or pathological lesion [72]. Indeed, hypometabolism has been shown to have stronger associations with amyloid-PET uptake in functionally connected regions than with local amyloid-PET uptake [73]. Here, we showed evidence of strong regional relationships between atrophy and hypometabolism in the Probable AD group when both modalities were assessed at baseline and M-12 follow-up visit as well as in the SNAP group at M-12 follow-up. While we did not directly assess tau pathology, this finding of a stronger spatial coupling of atrophy and hypometabolism in CSF tau-positive subjects is consistent with prior research suggesting that tau accumulation drives local neurodegeneration [64, 74]. It is important to note, however, that while measures of CSF p-tau are related to degree of tau-pathology as assessed by tau-PET, these effects are only moderate [75]. Atrophy-hypometabolism relationships that may suggest a focal disease process were only evident in our analyses among SNAP at M-12 and among Probable AD at baseline and M-12. Neurobiologically, we hypothesize that this may represent tau “driving” local neurodegeneration in these

groups at these time points, thus creating a signal that is both represented in, and correlated between, atrophy and hypometabolism. A logical next step for future research in this area would be to employ similar multivariate paradigms assessing concordance between atrophy and hypometabolism with tau and amyloid PET. If tau indeed drives local neurodegeneration in SNAP and other tau-positive groups, we may expect to find similar overlapping patterns of relationships among canonical dimensions between the two modalities. In contrast, we would expect to see spatially distant relationships between atrophy and amyloid-PET in both Amyloid Only and Probable AD groups.

Our investigation of between time-point relationships between atrophy and hypometabolism revealed topographically distinct relationships between modalities across groups. In particular, non-spatially overlapping but spatially contiguous relationships between atrophy and hypometabolism were consistently observed in the Amyloid Only group across the three sets of time points assessed. While we did not directly assess amyloid- β pathology using amyloid-PET, previous reports of amyloid-PET abnormalities in the absence of indicators of tau pathology have been shown have weak relationships with the patterns of neurodegeneration (atrophy/hypometabolism) and cognition [44, 76]. However, longitudinal studies of AD subjects suggest that amyloid- β and p-tau may act synergistically to trigger clinical disease progression [77, 78]. Indeed, while initial amyloid- β deposition occurs in the heteromodal association cortices [79], connectivity-mediated interactions between neurofibrillary tangles in the entorhinal cortex and distal amyloid- β may drive further tau spreading and concurrent neurodegeneration [80]. Consistent with these models, we observed relationships between atrophy and hypometabolism in tau-negative subjects which was sparse and typically restricted to lateral prefrontal regions at both baseline and between baseline and M-12 follow-up. At M-12 follow-up, canonical correlation analyses revealed patches of atrophy in the temporal lobe correlated with frontal lobe hypometabolism. Importantly, while Amyloid Only subjects in our study were p-tau negative as assessed by CSF, this does not necessarily preclude the possibility that these individuals harbor tau pathology, either at subthreshold levels or that tau-pathology was developed over the follow-up period.

SNAP subjects are an understudied, presumably heterogenous group of individuals [8–12]. Here, we

found minimal deviations from expected atrophy and hypometabolism in SNAP subjects at both baseline and M-12 follow-up visits. This is consistent with our prior study demonstrating minimal group-level differences with biomarker normal subjects in atrophy or hypometabolism among SNAP subjects within the ADNI cohort [24]. This may indicate that the present SNAP group may not reflect individuals with an active neurodegenerative process, as t-tau elevations denoting A/T/N “N” positivity are presumed to be nonspecific and can occur due to a number of non-neurodegenerative processes, including vascular insults, traumatic brain injury, or other medical comorbidities [81]. However, a significant portion of the SNAP subjects studied here had both t-tau and p-tau positivity and showed clinical disease severity scores similar to those in the Amyloid Only group (see Table 1 for sample characteristics). To that end, the SNAP group may represent individuals with non-Alzheimer’s neurodegenerative pathologies that are commonly observed in elderly or amyloid-negative cohorts, including α -synucleinopathies, non-Alzheimer tauopathies, TDP-43 proteinopathies, or vascular lesions [82, 83]. Postmortem neuropathological examinations reveal that SNAP have heterogeneous pathological profiles and are more likely to have mixed pathologies than amyloid-positive groups [84]. Moreover, the presence of both TDP-43 and tau pathology has been shown to correlate with hippocampal volume among SNAP subjects [84], offering a possible mechanistic role for the amnesic deficits observed in this group.

We observed atrophy-hypometabolism relationships in SNAP subjects which were topographically overlapping, similar to those in the Probable AD group, but at the M-12 follow-up visit only, i.e., as they progressed over time. Interestingly, W-scores within regions of ^{18}F FDG-PET hypometabolism and atrophy identified as correlated by the SCCA showed significant associations to longitudinal memory change in the SNAP group. These relationships were strongest within regions of ^{18}F FDG-PET hypometabolism at baseline that were identified as correlated to M-12 atrophy. Similarly, patches of ^{18}F FDG-PET hypometabolism identified as by the SCCA in the Probable AD group as related to longitudinal atrophy were similarly related to cognition. Thus, regions where ^{18}F FDG-PET hypometabolism is closely correlated to concurrent and future atrophy could possibly serve as a biomarker for tau-related neurodegeneration and help identify subjects at greatest risk for future cognitive decline. In both SNAP and

Probable AD, the SCCA-derived patches of ^{18}F FDG-PET hypometabolism that showed significant relationships to cognition were generally located in the bilateral temporal and parietal cortex, areas which are known to neuroanatomically subserve memory functions [85] and to degenerate in AD [86]. However, the SCCA-derived patches of atrophy identified in the SNAP group as correlated to longitudinal cognitive change were located in the posterior and anterior cingulate as well as prefrontal cortex. These areas may support memory [87] but also comprise portions of the salience network [88], which has been shown to selectively degenerate in non-AD neuropathologies, such as behavioral-variant frontotemporal dementia [1]. Future research should investigate whether regions identified by the present SCCA analyses are uniquely implicated in connectivity-based disease progression in this SNAP group.

Several considerations with regard to this work should be noted. First, our sample size was limited by the number of subjects from the ADNI cohort who had both a baseline and M-12 MRI and ^{18}F FDG-PET scan, and who additionally underwent CSF immunoassays at baseline. A restrictive number of subjects did not receive CSF immunoassays at their M-12 follow-up visit, and as such we do not know whether all our A/T/N subjects remained in the same category at their follow-up visit. Nevertheless, a considerable strength of the present analysis is the use of a longitudinal subject design. Studies that have previously examined multimodal correlations between imaging modalities have only done so within a single time point [22, 32], and few have examined these relationships both within and across time points within the A/T/N framework [89]. Regarding the A/T/N framework, while we have previously employed the this framework [24] to assess differences between SNAP and Alzheimer's Disease Continuum (AD-Continuum) subjects, the latter group contains any amyloid- β positive subject. It is likely that the AD-Continuum group is highly heterogenous with regard to clinical or cognitive severity, given that approximately one-third of cognitively normal older adults have AD pathology in their brains [90]. To this end, in the present study, we split the AD-Continuum group into Amyloid Only (e.g., A+T-N-) and Probable AD (A+T+N+) to better understand the differential effect of the presence of amyloid- β versus t-tau/p-tau biomarker positivity on atrophy-hypometabolism relationships.

The present study extends prior findings in several important ways. We found complex spatial associa-

tions between atrophy and glucose hypometabolism across three combinations of time points, that additionally differ based on the presence/absence of markers of amyloid- β and tau pathology in the CSF. As predicted, we observed less spatial overlap in the patches which contributed to the atrophy-hypometabolism relationship when baseline hypometabolism was correlated to atrophy at the M-12 follow-up visit. Further, non-spatially overlapping, but spatially contiguous, relationships between atrophy and hypometabolism were observed at all time points in the Amyloid Only group, possibly reflecting early amyloid deposition across heteromodal association cortices that is not yet associated with a tau-mediated neurodegenerative process in the medial temporal lobes. Finally, we observed strong spatial overlap in the atrophy-hypometabolism relationship in both the tau-positive SNAP and Probable AD groups, possibly reflecting tau-driven local neurodegeneration in the temporal cortices. Longitudinal multimodal neuroimaging studies such as these are incredibly valuable in the endeavor to characterize the trajectory of AD and non-AD neuropathological change and can aid in the detection of biomarkers for clinical decline.

ACKNOWLEDGMENTS

The authors have no acknowledgments to report.

FUNDING

This project was supported by R01-AG055121 from the National Institute on Aging.

CONFLICT OF INTEREST

The authors have no conflict of interest to report.

DATA AVAILABILITY

These data were derived from the following resources available in the public domain: <https://www.adni.loni.usc.edu>.

SUPPLEMENTARY MATERIAL

The supplementary material is available in the electronic version of this article: <https://dx.doi.org/10.3233/JAD-220975>.

REFERENCES

- [1] Seeley WW, Crawford RK, Zhou J, Miller BL, Greicius MD (2009) Neurodegenerative diseases target large-scale human brain networks. *Neuron* **62**, 42-52.
- [2] Jack Jr CR, Bennett DA, Blennow K, Carrillo MC, Dunn B, Haeberlein SB, Holtzman DM, Jagust W, Jessen F, Karlawish J (2018) NIA-AA research framework: Toward a biological definition of Alzheimer's disease. *Alzheimers Dement* **14**, 535-562.
- [3] Simonsen A, McGuire J, Podust V, Hagnelius N-O, Nilsson TK, Kapaki E, Vassilopoulos D, Waldemar G (2007) A novel panel of cerebrospinal fluid biomarkers for the differential diagnosis of Alzheimer's disease versus normal aging and frontotemporal dementia. *Dement Geriatr Cogn Disord* **24**, 434-440.
- [4] de Souza LC, Lamari F, Belliard S, Jardel C, Houllier C, De Paz R, Dubois B, Sarazin M (2011) Cerebrospinal fluid biomarkers in the differential diagnosis of Alzheimer's disease from other cortical dementias. *J Neurol Neurosurg Psychiatry* **82**, 240-246.
- [5] Caroli A, Frisoni G, Alzheimer's Disease Neuroimaging Initiative (2010) The dynamics of Alzheimer's disease biomarkers in the Alzheimer's Disease Neuroimaging Initiative cohort. *Neurobiol Aging* **31**, 1263-1274.
- [6] Jack CR, Vemuri J, Wiste HJ, Weigand SD, Aisen PS, Trojanowski JQ, Shaw LM, Bernstein MA, Petersen RC, Weiner MW (2011) Evidence for ordering of Alzheimer disease biomarkers. *Arch Neurol* **68**, 1526-1535.
- [7] Barber RC (2010) Biomarkers for early detection of Alzheimer disease. *J Am Osteopath Assoc* **110**, S10.
- [8] Caroli A, Prestia A, Galluzzi S, Ferrari C, Van Der Flier WM, Ossenkoppele R, Van Berckel B, Barkhof F, Teunissen C, Wall AE (2015) Mild cognitive impairment with suspected nonamyloid pathology (SNAP): Prediction of progression. *Neurology* **84**, 508-515.
- [9] Prestia A, Caroli A, Van Der Flier WM, Ossenkoppele R, Van Berckel B, Barkhof F, Teunissen CE, Wall AE, Carter SF, Schöll M (2013) Prediction of dementia in MCI patients based on core diagnostic markers for Alzheimer disease. *Neurology* **80**, 1048-1056.
- [10] Schreiber S, Schreiber F, Lockhart SN, Horng A, Bejanin A, Landau SM, Jagust WJ (2017) Alzheimer disease signature neurodegeneration and apoe genotype in mild cognitive impairment with suspected non-Alzheimer disease pathophysiology. *JAMA Neurol* **74**, 650-659.
- [11] Wisse L, Das S, Davatzikos C, Dickerson B, Xie S, Yushkevich P, Wolk D, Initiative AsDN (2018) Defining SNAP by cross-sectional and longitudinal definitions of neurodegeneration. *Neuroimage Clin* **18**, 407-412.
- [12] Wisse LE, Butala N, Das SR, Davatzikos C, Dickerson BC, Vaishnavi SN, Yushkevich PA, Wolk DA, Initiative AsDN (2015) Suspected non-AD pathology in mild cognitive impairment. *Neurobiol Aging* **36**, 3152-3162.
- [13] Dukart J, Kherif F, Mueller K, Adaszewski S, Schroeter ML, Frackowiak RS, Draganski B, Initiative AsDN (2013) Generative FDG-PET and MRI model of aging and disease progression in Alzheimer's disease. *PLoS Comput Biol* **9**, e1002987.
- [14] Heiss WD, Hilker R (2004) The sensitivity of 18-fluorodopa positron emission tomography and magnetic resonance imaging in Parkinson's disease. *Eur J Neurol* **11**, 5-12.
- [15] Jack Jr CR, Lowe VJ, Senjem ML, Weigand SD, Kemp BJ, Shiung MM, Knopman DS, Boeve BF, Klunk WE, Mathis CA (2008) 11C PiB and structural MRI provide complementary information in imaging of Alzheimer's disease and amnesic mild cognitive impairment. *Brain* **131**, 665-680.
- [16] Yuan Y, Gu Z-X, Wei W-S (2009) Fluorodeoxyglucose-positron-emission tomography, single-photon emission tomography, and structural MR imaging for prediction of rapid conversion to Alzheimer disease in patients with mild cognitive impairment: A meta-analysis. *Am J Neuroradiol* **30**, 404-410.
- [17] Frisoni GB, Fox NC, Jack CR, Scheltens P, Thompson PM (2010) The clinical use of structural MRI in Alzheimer disease. *Nat Rev Neurol* **6**, 67-77.
- [18] Jagust W (2006) Positron emission tomography and magnetic resonance imaging in the diagnosis and prediction of dementia. *Alzheimers Dement* **2**, 36-42.
- [19] Sperling RA, Aisen PS, Beckett LA, Bennett DA, Craft S, Fagan AM, Iwatsubo T, Jack CR, Jr., Kaye J, Montine TJ, Park DC, Reiman EM, Rowe CC, Siemers E, Stern Y, Yaffe K, Carrillo MC, Thies B, Morrison-Bogorad M, Wagster MV, Phelps CH (2011) Toward defining the preclinical stages of Alzheimer's disease: Recommendations from the National Institute on Aging-Alzheimer's Association workgroups on diagnostic guidelines for Alzheimer's disease. *Alzheimers Dement* **7**, 280-292.
- [20] Bejanin A, La Joie R, Landeau B, Belliard S, De La Sayette V, Eustache F, Desgranges B, Chételat G (2019) Distinct interplay between atrophy and hypometabolism in Alzheimer's versus semantic dementia. *Cereb Cortex* **29**, 1889-1899.
- [21] Whitwell JL, Graff-Radford J, Tosakulwong N, Weigand SD, Machulda MM, Senjem ML, Spychalla AJ, Vemuri P, Jones DT, Drubach DA (2018) Imaging correlations of tau, amyloid, metabolism, and atrophy in typical and atypical Alzheimer's disease. *Alzheimers Dement* **14**, 1005-1014.
- [22] Sintini I, Schwarz CG, Martin PR, Graff-Radford J, Machulda MM, Senjem ML, Reid RI, Spychalla AJ, Drubach DA, Lowe VJ (2019) Regional multimodal relationships between tau, hypometabolism, atrophy, and fractional anisotropy in atypical Alzheimer's disease. *Hum Brain Mapp* **40**, 1618-1631.
- [23] Villain N, Desgranges B, Viader F, De La Sayette V, Mézange F, Landeau B, Baron J-C, Eustache F, Chételat G (2008) Relationships between hippocampal atrophy, white matter disruption, and gray matter hypometabolism in Alzheimer's disease. *J Neurosci* **28**, 6174-6181.
- [24] Stocks J, Popuri K, Heywood A, Tosun D, Alpert K, Beg MF, Rosen H, Wang L, Initiative ftAsDN (2022) Network-wise concordance of multimodal neuroimaging features across the Alzheimer's disease continuum. *Alzheimers Dement (Amst)* **14**, e12304.
- [25] Fornito A, Zalesky A, Breakspear M (2015) The connectomics of brain disorders. *Nat Rev Neurosci* **16**, 159-172.
- [26] Benvenuto A, Giusiano B, Koric L, Gueriot C, Didic M, Felician O, Guye M, Guedj E, Ceccaldi M (2018) Imaging biomarkers of neurodegeneration in Alzheimer's disease: Distinct contributions of cortical MRI atrophy and FDG-PET hypometabolism. *J Alzheimers Dis* **65**, 1147-1157.
- [27] Borroni B, Premi E, Di Luca M, Padovani A (2007) Combined biomarkers for early Alzheimer disease diagnosis. *Curr Med Chem* **14**, 1171-1178.
- [28] Varma VR, Chuang Y-F, Thambisetty M (2020) Neuroimaging and fluid biomarkers of Alzheimer's disease: Implications for definition, diagnosis, and treatment. In *Oxford Textbook of Neurologic and Neuropsychiatric Epidemiology*, Brayne C, Feigin VL, Launer LJ, Logroscino G, eds. Oxford University Press, pp. 9-20.

- [29] Mutlu J, Landeau B, Gaubert M, de La Sayette V, Desgranges B, Chételat G (2017) Distinct influence of specific versus global connectivity on the different Alzheimer's disease biomarkers. *Brain* **140**, 3317-3328.
- [30] Jack CR Jr, Knopman DS, Jagust WJ, Shaw LM, Aisen PS, Weiner MW, Petersen RC, Trojanowski JQ (2010) Hypothetical model of dynamic biomarkers of the Alzheimer's pathological cascade. *Lancet Neurol* **9**, 119-128.
- [31] Gordon BA, Blazey TM, Su Y, Hari-Raj A, Dincer A, Flores S, Christensen J, McDade E, Wang G, Xiong C (2018) Spatial patterns of neuroimaging biomarker change in individuals from families with autosomal dominant Alzheimer's disease: A longitudinal study. *Lancet Neurol* **17**, 241-250.
- [32] Adams JN, Lockhart SN, Li L, Jagust WJ (2019) Relationships between tau and glucose metabolism reflect Alzheimer's disease pathology in cognitively normal older adults. *Cereb Cortex* **29**, 1997-2009.
- [33] Avants BB, Cook PA, Ungar L, Gee JC, Grossman M (2010) Dementia induces correlated reductions in white matter integrity and cortical thickness: A multivariate neuroimaging study with sparse canonical correlation analysis. *Neuroimage* **50**, 1004-1016.
- [34] Villain N, Fouquet M, Baron J-C, Mézence F, Landeau B, de La Sayette V, Viader F, Eustache F, Desgranges B, Chételat G (2010) Sequential relationships between grey matter and white matter atrophy and brain metabolic abnormalities in early Alzheimer's disease. *Brain* **133**, 3301-3314.
- [35] Jack Jr CR, Bernstein MA, Fox NC, Thompson P, Alexander G, Harvey D, Borowski B, Britson PJ, Whitwell LJ, Ward C (2008) The Alzheimer's disease neuroimaging initiative (ADNI): MRI methods. *J Magn Reson Imaging* **27**, 685-691.
- [36] Mueller SG, Weiner MW, Thal LJ, Petersen RC, Jack C, Jagust W, Trojanowski JQ, Toga AW, Beckett L (2005) The Alzheimer's disease neuroimaging initiative. *Neuroimaging Clin* **15**, 869-877.
- [37] Andreasen N, Sjøgren M, Blennow K (2003) CSF markers for Alzheimer's disease: Total tau, phospho-tau and A β 42. *World J Biol Psychiatry* **4**, 147-155.
- [38] Jack CR, Knopman DS, Chételat G, Dickson D, Fagan AM, Frisoni GB, Jagust W, Mormino EC, Petersen RC, Sperling RA (2016) Suspected non-Alzheimer disease pathophysiology—concept and controversy. *Nat Rev Neurol* **12**, 117-124.
- [39] Hansson O, Seibyl J, Stomrud E, Zetterberg H, Trojanowski JQ, Bittner T, Lifke V, Corradini V, Eichenlaub U, Batrla R (2018) CSF biomarkers of Alzheimer's disease concord with amyloid- β PET and predict clinical progression: A study of fully automated immunoassays in BioFINDER and ADNI cohorts. *Alzheimers Dement* **14**, 1470-1481.
- [40] Fischl B (2012) FreeSurfer. *Neuroimage* **62**, 774-781.
- [41] Lerch JP, Evans AC (2005) Cortical thickness analysis examined through power analysis and a population simulation. *Neuroimage* **24**, 163-173.
- [42] Jenkinson M, Bannister P, Brady M, Smith S (2002) Improved optimization for the robust and accurate linear registration and motion correction of brain images. *Neuroimage* **17**, 825-841.
- [43] Hagler DJ, Jr., Saygin AP, Sereno MI (2006) Smoothing and cluster thresholding for cortical surface-based group analysis of fMRI data. *Neuroimage* **33**, 1093-1103.
- [44] La Joie R, Perrotin A, Barré L, Hommet C, Mézence F, Ibazizene M, Camus V, Abbas A, Landeau B, Guilloteau D (2012) Region-specific hierarchy between atrophy, hypometabolism, and β -amyloid (A β) load in Alzheimer's disease dementia. *J Neurosci* **32**, 16265-16273.
- [45] Chételat G, Desgranges B, Landeau B, Mézence F, Poline J, de La Sayette V, Viader F, Eustache F, Baron J-C (2008) Direct voxel-based comparison between grey matter hypometabolism and atrophy in Alzheimer's disease. *Brain* **131**, 60-71.
- [46] Ma D, Popuri K, Bhalla M, Sangha O, Lu D, Cao J, Jacova C, Wang L, Beg MF, Initiative AsDN (2019) Quantitative assessment of field strength, total intracranial volume, sex, and age effects on the goodness of harmonization for volumetric analysis on the ADNI database. *Hum Brain Mapp* **40**, 1507-1527.
- [47] Popuri K, Balachandar R, Alpert K, Lu D, Bhalla M, Mackenzie IR, Hsiung RG, Wang L, Beg MF, Alzheimer's Disease Neuroimaging Initiative (2018) Development and validation of a novel dementia of Alzheimer's type (DAT) score based on metabolism FDG-PET imaging. *Neuroimage Clin* **18**, 802-813.
- [48] Glasser MF, Coalson TS, Robinson EC, Hacker CD, Harwell J, Yacoub E, Ugurbil K, Andersson J, Beckmann CF, Jenkinson M, Smith SM, Van Essen DC (2016) A multimodal parcellation of human cerebral cortex. *Nature* **536**, 171-178.
- [49] Hardoon DR, Szedmak S, Shawe-Taylor J (2004) Canonical correlation analysis: An overview with application to learning methods. *Neural Comput* **16**, 2639-2664.
- [50] Witten DM, Tibshirani RJ (2009) Extensions of sparse canonical correlation analysis with applications to genomic data. *Stat Appl Genet Mol Biol* **8**, Article28.
- [51] Mowinckel AM, Vidal-Piñeiro D (2020) Visualization of brain statistics with R packages ggseg and ggseg3d. *Adv Methods Pract Psychol Sci* **3**, 466-483.
- [52] Drost H-G (2018) Philentropy: Information theory and distance quantification with R. *J Open Source Softw* **3**, 765.
- [53] Crane PK, Carle A, Gibbons LE, Insel P, Mackin RS, Gross A, Jones RN, Mukherjee S, Curtis SM, Harvey D (2012) Development and assessment of a composite score for memory in the Alzheimer's Disease Neuroimaging Initiative (ADNI). *Brain Imaging Behav* **6**, 502-516.
- [54] Mosconi L (2005) Brain glucose metabolism in the early and specific diagnosis of Alzheimer's disease. *Eur J Nucl Med Mol Imaging* **32**, 486-510.
- [55] Hunt A, Schönknecht P, Henze M, Seidl U, Haberkorn U, Schröder J (2007) Reduced cerebral glucose metabolism in patients at risk for Alzheimer's disease. *Psychiatry Res Neuroimaging* **155**, 147-154.
- [56] Nestor PJ, Scheltens P, Hodges JR (2004) Advances in the early detection of Alzheimer's disease. *Nat Med* **10**, S34-S41.
- [57] Chételat G, Desgranges B, de la Sayette V, Viader F, Berkouk K, Landeau B, Lalevée C, Le Doze F, Dupuy B, Hannequin D (2003) Dissociating atrophy and hypometabolism impact on episodic memory in mild cognitive impairment. *Brain* **126**, 1955-1967.
- [58] Ishii K, Sasaki H, Kono AK, Miyamoto N, Fukuda T, Mori E (2005) Comparison of gray matter and metabolic reduction in mild Alzheimer's disease using FDG-PET and voxel-based morphometric MR studies. *Eur J Nucl Med Mol Imaging* **32**, 959-963.
- [59] Wei H, Kong M, Zhang C, Guan L, Ba M, Alzheimer's Disease Neuroimaging Initiative (2018) The structural MRI markers and cognitive decline in prodromal Alzheimer's disease: A 2-year longitudinal study. *Quant Imaging Med Surg* **8**, 1004.
- [60] Lehmann M, Douiri A, Kim LG, Modat M, Chan D, Ourselin S, Barnes J, Fox NC (2010) Atrophy patterns in

- Alzheimer's disease and semantic dementia: A comparison of FreeSurfer and manual volumetric measurements. *Neuroimage* **49**, 2264-2274.
- [61] Whitwell JL, Przybelski SA, Weigand SD, Knopman DS, Boeve BF, Petersen RC, Jack Jr CR (2007) 3D maps from multiple MRI illustrate changing atrophy patterns as subjects progress from mild cognitive impairment to Alzheimer's disease. *Brain* **130**, 1777-1786.
- [62] Cerami C, Crespi C, Della Rosa PA, Dodich A, Marcone A, Magnani G, Coppi E, Falini A, Cappa SF, Perani D (2015) Brain changes within the visuo-spatial attentional network in posterior cortical atrophy. *J Alzheimers Dis* **43**, 385-395.
- [63] La Joie R, Visani AV, Baker SL, Brown JA, Bourakova V, Cha J, Chaudhary K, Edwards L, Iaccarino L, Janabi M, Lesman-Segev OH, Miller ZA, Perry DC, O'Neil JP, Pham J, Rojas JC, Rosen HJ, Seeley WW, Tsai RM, Miller BL, Jagust WJ, Rabinovici GD (2020) Prospective longitudinal atrophy in Alzheimer's disease correlates with the intensity and topography of baseline tau-PET. *Sci Transl Med* **12**, eaau5732.
- [64] Iaccarino L, La Joie R, Edwards L, Strom A, Schonhaut DR, Ossenkoppele R, Pham J, Mellinger T, Janabi M, Baker SL (2021) Spatial relationships between molecular pathology and neurodegeneration in the Alzheimer's disease continuum. *Cereb Cortex* **31**, 1-14.
- [65] Morbelli S, Drzezga A, Perneczky R, Frisoni GB, Caroli A, van Berckel BN, Ossenkoppele R, Guedj E, Didic M, Brugnolo A (2012) Resting metabolic connectivity in prodromal Alzheimer's disease. A European Alzheimer Disease Consortium (EADC) project. *Neurobiol Aging* **33**, 2533-2550.
- [66] Rocher AB, Chapon F, Blaizot X, Baron J-C, Chavoix C (2003) Resting-state brain glucose utilization as measured by PET is directly related to regional synaptophysin levels: A study in baboons. *Neuroimage* **20**, 1894-1898.
- [67] Höglund K, Kern S, Zettergren A, Börjesson-Hansson A, Zetterberg H, Skoog I, Blennow K (2017) Preclinical amyloid pathology biomarker positivity: Effects on tau pathology and neurodegeneration. *Transl Psychiatry* **7**, e995-e995.
- [68] Spillantini MG, Goedert M (2013) Tau pathology and neurodegeneration. *Lancet Neurol* **12**, 609-622.
- [69] Bejanin A, Schonhaut DR, La Joie R, Kramer JH, Baker SL, Sosa N, Ayakta N, Cantwell A, Janabi M, Lauriola M (2017) Tau pathology and neurodegeneration contribute to cognitive impairment in Alzheimer's disease. *Brain* **140**, 3286-3300.
- [70] Taylor LM, McMillan PJ, Liachko NF, Strovast TJ, Ghetti B, Bird TD, Keene CD, Kraemer BC (2018) Pathological phosphorylation of tau and TDP-43 by TTBK1 and TTBK2 drives neurodegeneration. *Mol Neurodegener* **13**, 1-14.
- [71] Dronse J, Fliessbach K, Bischof GN, von Reutern B, Faber J, Hammes J, Kuhnert G, Neumaier B, Onur OA, Kukolja J (2017) *In vivo* patterns of tau pathology, amyloid- β burden, and neuronal dysfunction in clinical variants of Alzheimer's disease. *J Alzheimers Dis* **55**, 465-471.
- [72] Strom A, Iaccarino L, Edwards L, Lesman-Segev OH, Soleimani-Meigooni DN, Pham J, Baker SL, Landau SM, Jagust WJ, Miller BL (2022) Cortical hypometabolism reflects local atrophy and tau pathology in symptomatic Alzheimer's disease. *Brain* **145**, 713-728.
- [73] Pascoal TA, Mathotaarachchi S, Kang MS, Mohaddes S, Shin M, Park AY, Parent MJ, Benedet AL, Chamoun M, Theriault J (2019) A β -induced vulnerability propagates via the brain's default mode network. *Nat Commun* **10**, 1-13.
- [74] Iaccarino L, Tammewar G, Ayakta N, Baker SL, Bejanin A, Boxer AL, Gorno-Tempini ML, Janabi M, Kramer JH, Lazaris A (2018) Local and distant relationships between amyloid, tau and neurodegeneration in Alzheimer's Disease. *Neuroimage Clin* **17**, 452-464.
- [75] La Joie R, Bejanin A, Fagan AM, Ayakta N, Baker SL, Bourakova V, Boxer AL, Cha J, Karydas A, Jerome G (2018) Associations between [18F] AV1451 tau PET and CSF measures of tau pathology in a clinical sample. *Neurology* **90**, e282-e290.
- [76] Ossenkoppele R, Schonhaut DR, Schöll M, Lockhart SN, Ayakta N, Baker SL, O'Neil JP, Janabi M, Lazaris A, Cantwell A (2016) Tau PET patterns mirror clinical and neuroanatomical variability in Alzheimer's disease. *Brain* **139**, 1551-1567.
- [77] Weiner MW, Veitch DP, Aisen PS, Beckett LA, Cairns NJ, Green RC, Harvey D, Jack Jr CR, Jagust W, Morris JC (2017) Recent publications from the Alzheimer's Disease Neuroimaging Initiative: Reviewing progress toward improved AD clinical trials. *Alzheimers Dement* **13**, e1-e85.
- [78] Busche MA, Hyman BT (2020) Synergy between amyloid- β and tau in Alzheimer's disease. *Nat Neurosci* **23**, 1183-1193.
- [79] Thal DR, Rüb U, Orantes M, Braak H (2002) Phases of A β -deposition in the human brain and its relevance for the development of AD. *Neurology* **58**, 1791-1800.
- [80] Lee WJ, Brown JA, Kim HR, La Joie R, Cho H, Lyoo CH, Rabinovici GD, Seong J-K, Seeley WW, Alzheimer's Disease Neuroimaging Initiative (2022) Regional A β -tau interactions promote onset and acceleration of Alzheimer's disease tau spreading. *Neuron* **110**, 1932-1943.e5.
- [81] Soldan A, Pettigrew C, Fagan AM, Schindler SE, Moghekar A, Fowler C, Li Q-X, Collins SJ, Carlsson C, Asthana S (2019) ATN profiles among cognitively normal individuals and longitudinal cognitive outcomes. *Neurology* **92**, e1567-e1579.
- [82] Kovacs GG, Milenkovic I, Wöhrer A, Höftberger R, Gelpi E, Haberler C, Hönigschnabl S, Reiner-Concin A, Heinzl H, Jungwirth S (2013) Non-Alzheimer neurodegenerative pathologies and their combinations are more frequent than commonly believed in the elderly brain: A community-based autopsy series. *Acta Neuropathol* **126**, 365-384.
- [83] Chételat G, Ossenkoppele R, Villemagne VL, Perrotin A, Landeau B, Mézenge F, Jagust WJ, Dore V, Miller BL, Egret S (2016) Atrophy, hypometabolism and clinical trajectories in patients with amyloid-negative Alzheimer's disease. *Brain* **139**, 2528-2539.
- [84] Wisse L, de Flores R, Xie L, Das S, McMillan C, Trojanowski J, Grossman M, Lee E, Irwin D, Yushkevich P (2021) Pathological drivers of neurodegeneration in suspected non-Alzheimer's disease pathophysiology. *Alzheimers Res Ther* **13**, 1-11.
- [85] Alvarez P, Squire LR (1994) Memory consolidation and the medial temporal lobe: A simple network model. *Proc Natl Acad Sci U S A* **91**, 7041-7045.
- [86] Chan D, Fox NC, Scahill RI, Crum WR, Whitwell JL, Leschziner G, Rossor AM, Stevens JM, Cipelotti L, Rossor MN (2001) Patterns of temporal lobe atrophy in semantic dementia and Alzheimer's disease. *Ann Neurol* **49**, 433-442.

- [87] Weible AP (2013) Remembering to attend: The anterior cingulate cortex and remote memory. *Behav Brain Res* **245**, 63-75.
- [88] Seeley (2019) The salience network: A neural system for perceiving and responding to homeostatic demands. *J Neurosci* **39**, 9878-9882.
- [89] Sintini I, Martin PR, Graff-Radford J, Senjem ML, Schwarz CG, Machulda MM, Spychalla AJ, Drubach DA, Knopman DS, Petersen RC (2019) Longitudinal tau-PET uptake and atrophy in atypical Alzheimer's disease. *Neuroimage Clin* **23**, 101823.
- [90] Bennett D, Schneider J, Arvanitakis Z, Kelly J, Aggarwal N, Shah R, Wilson R (2006) Neuropathology of older persons without cognitive impairment from two community-based studies. *Neurology* **66**, 1837-1844.